



Full Text View

[Volume 29, Issue 5 \(May 1999\)](#)

Journal of Physical Oceanography

 Article: pp. 911–924 | [Abstract](#) | [PDF \(211K\)](#)

Influence of a Strong Bottom Slope on the Evolution of a Surface-Intensified Vortex

Virginie Thierry

IFREMER-LPO, Plouzané, France

Yves Morel

EPSHOM-CMO, Brest, France

(Manuscript received September 25, 1997, in final form June 1, 1998)

DOI: 10.1175/1520-0485(1999)029<0911:IOASBS>2.0.CO;2

ABSTRACT

The authors investigate the influence of steep bottom topography on the propagation of a vortex in a two-layer quasigeostrophic model. The vortex is intensified in the upper layer and the planetary beta effect is taken into account.

The authors find that steep topography can scatter disturbances created by the upper-layer vortex displacement and maintain the lower-layer motion weak. It is thus shown that, when the vortex radius is smaller than a critical value, the vortex behaves as if the lower layer was at rest (or infinitely deep as in a reduced gravity model). If the radius is increased while holding the maximum vorticity of the vortex, the topographic Rossby waves—generated during the scattering process—have a stronger signature in the upper layer, and the vortex evolution begins to change in comparison with the reduced-gravity case. However, numerical experiments show that both the steep topography and reduced-gravity trajectories remain close up to a large radius, after which a vortex above a strong slope becomes unstable and is dispersed by topographic Rossby waves.

1. Introduction

In so far as displacement, merging, or stability is concerned, barotropic¹ and baroclinic vortices have very different behaviors (see [Flierl 1988](#); [Verron and Valcke 1994](#); [Reznik and Dewar 1994](#); [Sutyrin and Flierl 1994](#)). Because of their

Table of Contents:

- [Introduction](#)
- [Model](#)
- [Scaling analysis](#)
- [Reduced-gravity regime](#)
- [Regime limits](#)
- [Discussion](#)
- [REFERENCES](#)
- [APPENDIX](#)
- [FIGURES](#)

Options:

- [Create Reference](#)
- [Email this Article](#)
- [Add to MyArchive](#)
- [Search AMS Glossary](#)

Search CrossRef for:

- [Articles Citing This Article](#)

Search Google Scholar for:

- [Virginie Thierry](#)
- [Yves Morel](#)

relative simplicity, reduced-gravity models have often been used in both numerical and theoretical studies (Nof 1981; Killworth 1983), but, since the barotropic mode is filtered out from these models (the vertically averaged streamfunction is zero as the fluid is considered infinitely deep), some theoretical results are very sensitive to this assumption of no deep flow (Mory 1985; Mory et al. 1987; Flierl 1984; Swaters and Flierl 1991; Verron and Valcke 1994), and one may wonder if reduced-gravity models are relevant for oceanic processes.

Chassignet and Cushman-Roisin (1991) addressed this issue in a two-layer shallow-water model for the propagation of a vortex on the beta plane. They found that for the reduced-gravity model to be valid, the lower layer must be “deeper by a factor of 10 or so” than the upper layer and that either the vortex radius must be smaller than an internal radius of deformation or bigger than a beta-based radius. However, they did not take into account the effect of a bottom topography in their theoretical and numerical calculations.

It has been shown that when a vortex evolves on the planetary beta plane, it rapidly loses its coherence and is dispersed into Rossby waves if its potential vorticity anomaly gradient is less than β , where β is the planetary potential vorticity gradient (Flierl 1977; McWilliams and Flierl 1979). In this study, we focus on the behavior of surface intensified vortices above steep bottom topography. Thus, if the lower-layer background gradient of potential vorticity, which is proportional to the bottom slope, is stronger than the gradient of potential vorticity anomaly, the initial lower-layer velocity field is rapidly dispersed by the bottom topography (the time period for dispersion is inversely proportional to the bottom slope). On the f plane, La Casce (1998) showed that the end state is a structure with no motion in the lower layer and a circulation in the upper layer such that the potential vorticity anomaly has the same structure as initially. When the planetary beta effect is taken into account, the upper-layer vortex will develop a dipolar component, called beta gyre (see McWilliams and Flierl 1979; Sutyrin and Flierl 1994), leading to a displacement of the upper-layer structure that is no longer stationary. This stretches the deep-water columns and develops a motion in the lower layer. If it is not too strong, this motion is again subject to topographic dispersion. Kamenkovich et al. (1996) indeed found that when crossing a steep ridge, even large vortices such as Agulhas eddies become compensated.

There are thus some reasons to believe that, even when the beta effect is taken into account, steep bottom topography can maintain the lower-layer motion weak enough so that it can be considered at rest and that a surface intensified vortex could behave as in a reduced-gravity model.

The problem we address here is to seek under which conditions of background stratification and vortex characteristics the reduced-gravity model is valid when we take into account the dispersive effect associated with a strong bottom topography. The model is described in the second section. A scaling analysis is performed in the third section and yields some theoretical grounds that are used to explain our numerical experiments (presented in the fourth and fifth sections). Application to oceanic vortices is discussed in the last section.

2. Model

a. Quasigeostrophic equations

In this paper, we consider a two-layer quasigeostrophic (QG) model on the β plane and take into account the effect of a bottom topography with a constant slope (see Fig. 1). When the fluid is at rest, the first layer depth is H_1 and the second layer depth is $H_2 - s_x x - s_y y$, where (s_x, s_y) are the east–west and north–south slope components, respectively, and $s = (s_x^2 + s_y^2)^{1/2}$ is the bottom slope. The densities are ρ_1 and ρ_2 respectively, the Coriolis frequency is f , and the gravitational acceleration is g .

The inviscid equations rely on the conservation of the total potential vorticity in each layer and can be written (see Pedlosky 1987, chapter 6)

$$\begin{aligned} \frac{d}{dt}\Pi_k &= \partial_t \pi_k + J(\psi_k, \pi_k) + \beta_{k,y} \partial_x \psi_k - \beta_{k,x} \partial_y \psi_k = 0, \\ k &= 1, 2, \end{aligned} \quad (1)$$

where

$$\pi_1 = \zeta + F_1(\psi_2 - \psi_1) = \nabla^2 \psi_1 + F_1(\psi_2 - \psi_1) \quad (2a)$$

$$\pi_2 = \zeta + F_2(\psi_1 - \psi_2) = \nabla^2 \psi_2 + F_2(\psi_1 - \psi_2) \quad (2b)$$

is the potential vorticity anomaly in each layer and

$$\Pi_k = \pi_k + \beta_{k,x}x + \beta_{k,y}y \quad (3)$$

is the total potential vorticity.

In these equations $F_1 = f^2/g'H_1$, $F_2 = f^2/g'H_2$ with $g' = g(\rho_2 - \rho_1)/\rho_1$; $\beta_{1,y} = \beta$, $\beta_{1,x} = 0$; $\beta_{2,y} = \beta + fs_y/H_2$; $\beta_{2,x} = fs_x/H_2$, and β is the gradient of the planetary vorticity; $\beta_2 = (\beta_{2,x}^2 + \beta_{2,y}^2)^{1/2}$ then measures the background potential vorticity gradient in the second layer and will be used to evaluate topographic dispersion. Also Ψ_k is the streamfunction in layer k , $J(A, B) = \partial_x A \partial_y B - \partial_y A \partial_x B$ is the Jacobian operator, and $\zeta = \nabla^2 \Psi$ is the relative vorticity.

b. Numerical model

The numerical model we use is a pseudospectral code in the horizontal (a biperiodic domain with a 128×128 horizontal grid; [Orszag 1971](#)). A biharmonic viscosity is used with a viscosity coefficient $\nu = 5 \times 10^7$ to $5 \times 10^8 \text{ m}^4 \text{ s}^{-1}$ to avoid computational instability. The mesh size is $dx = 20R/128$ and depends on the vortex radius R (defined below). The time step is 2160 s, and the model is typically run for 150 days.

On the planetary beta plane, the vortex usually does not interact with the periodic continuation of the Rossby wave wake generated during its propagation within this time period. But for strong bottom slopes, the topographic Rossby waves rapidly crosses the domain and may interact with the vortex again. However, we believe that this does not alter our conclusions as different slope orientations do not seem to change the general vortex behavior.

c. Initial state, vortex structure

In this study we focus on vortices with a strong signature in the upper layer. We thus choose the initial streamfunctions as follows:

$$\psi_1 = \frac{\Omega_1 R^2}{2} e^{-r^2/2R^2},$$

where R is the vortex lengthscale and corresponds to the radius at which the velocity reaches its maximum, r is the distance from the vortex center, and $\Omega_1/2$ its rotation rate near the center. As we only consider anticyclonic vortices, Ω_1 is positive. Notice that the initial minimum vorticity $\zeta_1 = \nabla^2 \psi_1$ is $-\Omega_1$ (and not $-\Omega_1/2$).

To test for the sensitivity of the processes to vortex structure, we have considered vortices for which $\psi_2 = 0$ initially (so that the lower layer was initially at rest) and vortices with no initial potential vorticity anomaly in the second layer, $\pi_2 = 0$. On the f or β plane, many studies have shown that these structures usually have a very different behavior (see [Verron and Valcke 1994](#); [Morel and McWilliams 1997](#)). In addition to considering different initial deep flow, we have also tested for the sensitivity of our results to different slope orientations. The $\psi_2 = 0$ and $\pi_2 = 0$ cases have thus been systematically considered with different (s_x, s_y) couples (but the same bottom slope s) including east–west, north–south, or opposite sign slopes.

3. Scaling analysis

a. Process

As mentioned in the introduction, steep bottom topography is likely to maintain the lower-layer motion weak enough so that the upper-layer vortex evolves as in a reduced-gravity model. The bottom layer may however affect the general behavior and trajectory of the structure if either the lower-layer motion becomes strong enough so that the circulation it generates in the upper layer via stretching is comparable to the beta gyre or if the excitation of the topographic Rossby waves associated with the vortex displacement induces a strong energy leakage. If this latter and the second-layer motion are weak, the lower layer does not play a big role on the dynamics of the vortex, and it behaves as if the lower layer was at rest, or infinitely deep as in a reduced-gravity model.

In the following analysis, we address this issue assuming that the upper-layer vortex displacement is not affected by the topographic Rossby waves and behaves as if the lower layer was infinitely deep. We can then calculate the effect of the vortex displacement on the lower layer, and this yields an estimate of the lower-layer motion that can then be used to evaluate its influence on the development of the upper-layer beta gyre. We then seek a contradiction with the initial assumption (negligible effect of the lower layer) to derive an analytic criterion for the validity of the model.

b. Analysis

Let us develop [Eq. \(1\)](#) and derive a scaling for each term. The equation for the upper and lower layers can be written

$$\begin{aligned} & \underbrace{\partial_t(\zeta_1 - F_1\psi_1)}_{\text{T1}} + \underbrace{F_1\partial_t\psi_2}_{\text{T2}} + \underbrace{J(\psi_1, \zeta_1)}_{\text{T3}} + \underbrace{F_1J(\psi_1, \psi_2)}_{\text{T4}} \\ & + \underbrace{\beta_1\partial_x\psi_1}_{\text{T5}} = 0 \end{aligned} \quad (4a)$$

$$\begin{aligned} & \underbrace{\partial_t(\zeta_2 - F_2\psi_2)}_{\text{T6}} + \underbrace{F_2\partial_t\psi_1}_{\text{T7}} + \underbrace{J(\psi_2, \zeta_2)}_{\text{T8}} + \underbrace{F_2J(\psi_2, \psi_1)}_{\text{T9}} \\ & + \underbrace{\beta_{2,y}\partial_x\psi_2 - \beta_{2,x}\partial_y\psi_2}_{\text{T10}} = 0. \end{aligned} \quad (4b)$$

In [\(4a\)](#), if ψ_2 is weak enough, T2 and T4 are negligible and the equation is then equivalent to a reduced-gravity model on the β plane with an internal radius of deformation $R_1 = 1/F_1^{1/2}$. In this case, an intense upper-layer vortex keeps its axisymmetric part and translates essentially westward (see [Sutyrin and Flierl 1994](#)). This displacement is due to the development of a dipolar circulation component ψ'_1 called beta gyre and can be evaluated together with the propagation speed $C = R/\tau_1$ as T1, T3, and T5 have the same order of magnitude (see [McWilliams and Flierl 1979](#); [Sutyrin and Flierl 1994](#); [Reznik and Dewar 1994](#); [Sutyrin and Morel 1997](#)). At first, since T1 is associated with the axisymmetric part displacement, $O(\text{T1}) \approx CO(\nabla\pi_1)$. In the vortex core, both the stretching and relative vorticity terms have the same sign (negative for an anticyclone), and we can thus evaluate the order of magnitude of the potential vorticity anomaly π_1 by simply summing the order of magnitude of both terms. This yields $O(\text{T1}) \approx \Omega_1(1 + \frac{1}{2}F_1R^2)/\tau_1$. (Notice the $\frac{1}{2}$ coefficient for the order of magnitude of the stretching term. This coefficient depends, in fact, on the shape of the streamfunction but is usually close to $\frac{1}{2}$ when R is defined as the radius where the velocity is maximum.) Concerning T3, as the Jacobian term is zero for a purely axisymmetric structure, we must take into account the beta gyre component ψ'_1 to evaluate this nonlinear term. We get $O(\text{T3}) \approx \psi'_1\Omega_1/R^2$. The last term represents advection of background potential vorticity by the vortex circulation and a rough estimate is $O(\text{T5}) \approx \beta_1R\Omega_1/2$. As each term has the same order of magnitude, we finally get

$$\tau_1 \approx \frac{2 + F_1R^2}{\beta_1R}$$

$$\psi'_1 \approx \beta_1R^3/2.$$

Let us now consider [\(4b\)](#) and the lower-layer dynamics. As Rossby waves propagate along lines of constant total potential vorticity, dispersion occurs in this layer when potential vorticity contours extend to infinity. In our configuration, this happens when the order of magnitude of the background potential vorticity gradient $\beta_2 = (\beta_{2,x}^2 + \beta_{2,y}^2)^{1/2}$ ($\approx fs/H_2$ for a steep enough bottom topography) is greater than the potential vorticity anomaly gradient $\|\nabla\pi_2\|$. This condition yields a constraint on the upper-layer vortex strength (considering that the order of magnitude of π_2 is mainly given by $F_2\psi'_1$)

This parameter controls dispersion at depth and, in practice, rapid scattering occurs for values of δ_{disp} above 1 (up to $\delta_{\text{disp}} \approx 2$ or so). In this case, the nonlinear terms T8 + T9 (associated with the second-layer potential vorticity gradient) can be neglected in comparison with T10 (associated with the background gradient of potential vorticity). On the f plane this sole criterion governs the vortex evolution: if it is satisfied, the vortex becomes compensated (see [La Casce 1998](#)). On the beta plane, the upper vortex propagates and this induces a motion at depth through term T7, which acts as a forcing in (4b). To evaluate the order of magnitude of the circulation in the second layer we assume that δ_{disp} is small enough to neglect T8 and T9 in (4b) (see appendix A). We find that ψ_2 can be decomposed into two terms evolving at two different timescales: a slow one, $\tau_1 = (2 + F_1 R^2)/\beta_1 R$, associated with the upper-layer forcing, and a rapid one, $\tau_2 = (2 + F_2 R^2)/\beta_2 R$, associated with the topographic scattering. Both parts have the same order of magnitude for the lower-layer vorticity (see appendix A); it can also be obtained if we notice that T10 and T7 must have the same order of magnitude (they are both prevailing terms for the slow part). We get

$$O(\zeta_2) = \Omega_2 \approx \frac{F_2 \Omega_1 R}{\beta_2 \tau_1} = \frac{\beta_1}{\beta_2} \frac{F_2 R^2}{1 + F_1 R^2} \Omega_1. \quad (5)$$

When the vortex has an initial deep flow (for instance, when we choose $\pi_2 = 0$ initially), this scaling is, of course, not valid as long as the lower-layer motion has not been dissipated by the topographic Rossby waves. But this only lasts for a short time period of several τ_2 .

c. Criteria for model validity

We now evaluate the influence of the lower-layer circulation on the upper-layer vortex evolution and look for a contradiction with the previous hypothesis (negligible influence). This circulation changes the first-layer velocity and potential vorticity fields via stretching. In (4a) the second term is mainly associated with the fast topographic wave part of ψ_2 ($\tau_2 \ll \tau_1$) and represents the signature of the topographic Rossby waves in the first layer. Its ratio with T5 compares the topographic Rossby waves signature with the development of the beta gyre and will be called δ_{TRW} :

$$\begin{aligned} \delta_{\text{TRW}} &= \frac{O(\text{T2})}{O(\text{T5})} \simeq \frac{F_1 \Omega_2}{\tau_2 \beta_1 \Omega_1 R} \\ &= \frac{F_1 R^2 F_2 R^2}{(2 + F_1 R^2)(2 + F_2 R^2)}. \end{aligned} \quad (6a)$$

The fourth term is associated with the changes in the potential vorticity distribution due to the lower-layer circulation and subsequent interface deviation. It is a nonlinear effect, and its ratio with T5 will be called δ_{NL} :

$$\delta_{\text{NL}} = \frac{O(\text{T4})}{O(\text{T5})} \simeq \frac{F_1 R^2 \Omega_2}{\beta_1 R} = \frac{F_1 R^2}{1 + F_1 R^2} \frac{F_2 R^2 \Omega_1}{\beta_2 R}. \quad (6b)$$

The criteria for the validity of the reduced-gravity model are thus $\delta_{\text{disp}} < 1$, $\delta_{\text{TRW}} \ll 1$ and $\delta_{\text{NL}} \ll 1$.

4. Reduced-gravity regime

a. Dissipation

Let us imagine twin experiments with a vortex of the same initial shape in the upper layer, but a resting infinite lower layer on the one hand and a finite lower layer but with steep topography on the other hand. For the latter case, when δ_{TRW} and δ_{NL} are small, the topographic Rossby wave signature and the potential vorticity changes associated with the lower-layer motion (terms T2 and T4) can, a priori, be neglected in [Eq. \(4a\)](#) and the vortex in the first layer should evolve as if the lower layer was at rest. Thus, both experiments should yield the same evolution for the vortex in the first layer.

In fact, some discrepancies may appear because in the finite depth case, the upper-layer vortex displacement generates a motion in the lower layer that is associated with a significant energy loss on a long timescale. Thus some differences of the vortex strength and shape appear between both experiments after a while. To keep the same evolution, one must reinitialize the reduced-gravity experiment using the fields of the finite depth one with a period much shorter than the timescale associated with the decay due to the generation of bottom motion.

We have not been able to calculate the rate of decay (an estimation can however be given under some assumptions; see appendix B), but the numerical experiments seem to show that, in the reduced-gravity regime (δ_{NL} and δ_{TRW} small), it has little influence on the vortex evolution for the period of time considered in this paper (~ 150 days).

b. Flat bottom

If there is no bottom topography, dispersion in the lower layer can only happen if $\delta_{\text{disp}} = F_2 \Omega_1 R / \beta \lesssim 1$, where $\beta \approx 2 \times 10^{-11} \text{ m}^{-1} \text{ s}^{-1}$ is the planetary beta. On the other hand, for the vortex in the first layer to resist dispersion and stay coherent, a similar scaling analysis can be performed, which yields $\delta'_{\text{disp}} = F_1 \Omega_1 R / \beta \gg 1$. So both criteria can only be satisfied if $F_2 / F_1 = H_1 / H_2 \ll 1$.

This condition was first derived by [Chassignet and Cushman-Roisin \(1991\)](#), in the framework of a more general two-layer shallow-water model on the beta plane. They concluded that two conditions must be satisfied for the reduced-gravity model to be valid.


1. $F_2 / F_1 \ll 1$: the lower layer must be much bigger, by a factor of 10 or so, than the upper one.
2. $\min(F_1 R^2 F_2 R^2, F_2 \Omega_1 R / \beta) \ll 1$: the vortex radius is either smaller than an internal deformation radius or smaller than a beta-based horizontal scale.

Some slight differences exist between their results and the model developed in this paper due to different scaling analysis. For instance, Chassignet and Cushman-Roisin concluded, in fact, that when the radius of the vortex is *greater* than a beta-based critical radius, the reduced-gravity model can recover its validity; but in their model they chose to hold the maximum depth deviation (or streamfunction maximum $\Psi_{\text{max}} = R^2 \Omega_1 / 2$) constant while varying the vortex radius. This conclusion is changed if one chooses to test for the sensitivity of the vortex evolution to its radius with a fixed maximum velocity, potential vorticity anomaly, or, as is the case in this paper, fixed relative vorticity maximum Ω_1 . Both our and the Chassignet–Cushman-Roisin analysis however give the same order of magnitude for the validity of the reduced-gravity model (replacing Ω_1 by $2\Psi_{\text{max}}/R^2$). We will thus not compare both models further and focus on the additional effect of steep topography.

c. Sloping bottom case

When steep bottom topography is taken into account, the validity domain of the reduced-gravity regime is drastically changed. According to our scaling analysis, the bottom layer no longer needs to be much deeper than the upper one as steep topography is able to disperse the motion in the lower layer while keeping the upper-layer vortex coherent. Indeed, as β_2 depends on both the planetary beta and bottom slope, δ_{disp} can be greatly decreased if a steep slope is taken into account.

Let us first present an experiment with two layers of the same depth, for which Chassignet and Cushman-Roisin's constraint is not satisfied. For this preliminary experiment, we have chosen $H_1 = H_2 = 1500 \text{ m}$, $f = 7 \times 10^{-5} \text{ s}^{-1}$, $\beta = 2 \times 10^{-11} \text{ m}^{-1} \text{ s}^{-1}$, $g' = 0.01$, and a vortex with a maximum vorticity $\Omega_1 = 0.3f$ and a radius $R = 40 \text{ km}$. The lower layer is initially at rest. Such a vortex is able to resist dispersion in the upper layer ($\delta'_{\text{disp}} = F_1 \Omega_1 R / \beta \approx 15$) while the lower layer is subject to dispersion when a bottom slope $s = 0.01$ is taken into account ($\delta_{\text{disp}} = F_2 \Omega_1 R H_2 / f s \approx 0.8$). In addition, in this parameter regime, the reduced-gravity model should be valid (we get $\delta_{\text{TRW}} \approx 0.04$ and $\delta_{\text{NL}} \approx 0.1$).

[Figure 2](#)  represents the vortex trajectories on the beta plane with and without bottom slope and compared to a reduced-gravity model (plain). The duration of each simulation is 150 days. Two different bottom slope orientations are presented: the dashed trajectory corresponds to the $(s, s) = (0, 0.01)$ case (north–south slope) and circles to the $(s, s) =$



(0.01, 0) case (east–west orientation). Initially, $\psi_2 = 0$ and the dotted line is associated with the flat bottom experiment.

Even though some discrepancies appear after 80 days or so, the reduced-gravity model and the strong bottom slope cases yield comparable trajectories, whereas without topography the vortex displacement is quite different. Notice for instance how the trajectories are deviated westward in the reduced-gravity and strong slope cases. This is, in addition, independent of the slope orientation. The differences after 80 days are probably due to the energy loss associated with the development of motion in the lower layer for the finite depth case and we believe they can be avoided if the reduced-gravity model is reinitialized with the finite depth ψ_1 every 50 days in this case (the rate of decay calculated in appendix B yields $T_{\text{decay}} \approx 600$ days).

5. Regime limits




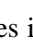


a. Reduced-gravity regime

Let us now consider a more “realistic” two-layer configuration with the following characteristics: $H_1 = 500$ m, $H_2 = 3500$ m, $g' = 0.01$ m s⁻², $f = 7 \times 10^{-5}$ s⁻¹ and $\beta = 2 \times 10^{-11}$ m⁻¹ s⁻¹. The internal radius of deformation is $R_d \approx 30$ km. We take a bottom slope $s = 0.015$ into account, the vortex maximum vorticity is $\Omega_1 = 0.3f$ and is held constant, but the radius R is now variable.

[Figure 3](#)  represents δ_{disp} as a function of the vortex radius. It shows that dispersion can occur in the lower layer for up to $R = 100$ km. [Figure 4](#)  shows δ_{TRW} (dashed) and δ_{NL} (plain) as a function of the vortex radius R . It shows that the reduced-gravity regime should be valid up to $R \approx 30$ km or so (δ_{TRW} and $\delta_{\text{NL}} \lesssim 0.1$). It is, in fact, rather difficult to estimate the largest value for which the reduced-gravity model and the finite depth/strong slope one give similar vortex evolution, as our criteria are based on a scaling analysis, not exact analytical calculations, and the discrepancies between both models cannot be evaluated. We have thus performed many experiments with different background stratification and found that, for the period of time considered here (150 days), both models roughly yield the same evolution if δ_{TRW} and δ_{NL} are both smaller than 0.3. Beyond this value, because of growing influence of the topographic Rossby waves in the upper layer, some discrepancies appear: the vortex shapes become different, and we observe a growing influence of the vortex initial deep flow (i.e., discrepancies appear between the $\psi_2 = 0$ and $\pi_2 = 0$ cases). The latter can, in fact, be explained if we consider the upper-layer potential vorticity. The $\psi_2 = 0$ and the $\pi_2 = 0$ initialization yields, indeed, very different Π_1 when the vortex radius becomes large. As this quantity is conserved and is important for the upper-vortex evolution, it is not really surprising to see growing influence of the initial deep flow when R is large.

It is however worth mentioning that as long as $\delta_{\text{NL}} \lesssim 1$ or so, both the reduced-gravity model and the steep topography case yield similar evolutions in the sense that in both models the meridional displacement is weak and the trajectories are close, whereas in the finite depth/flat bottom case, the southward displacement is as large as the westward displacement and the translation speed is much more important. In addition, the vortex often exhibits several instability periods above a flat bottom but remains stable above a steep topography or in a reduced-gravity model. Thus, in this intermediate parameter regime ($0.3 \lesssim \delta_{\text{NL}} \lesssim 1$), a vortex above a strong bottom slope appears to be trapped and to keep its signature in comparison with the flat bottom case (see [Thierry 1996](#)).

To illustrate these results, let us now compare the behavior of vortices in the reduced-gravity model to evolutions in the finite depth case with $H_1 = 500$ m, $H_2 = 3500$ m, $g' = 0.01$ m s⁻², different bottom topographies, and initial lower-layer streamfunction.

[Figures 5](#) , [6](#) , and [7](#)  represent the trajectories of the vortices in the reduced-gravity model (plain), with a finite depth without topography and $\psi_2 = 0$ (dotted) initially and with a finite depth but a strong north–south slope $(s_x, s_y) = (0, 0.015)$ and either $\psi_2 = 0$ (dashed) or $\pi_2 = 0$ (dash-dotted) initially. As mentioned previously, a different slope orientation $(s_x, s_y) = (0.015, 0)$ was also considered with the $\psi_2 = 0$ initialization, and the corresponding trajectory is represented by circles. The results are given for three different vortex radii $R = 30$ km ([Fig. 5](#) ) , $R = 40$ km ([Fig. 6](#) ) , $R = 80$ km ([Fig. 7](#) ) corresponding, respectively, to $(\delta_{\text{disp}}, \delta_{\text{TRW}}, \delta_{\text{NL}}) \approx (0.3, 0.08, 0.1)$, $(0.4, 0.18, 0.2)$, and $(0.8, 0.5, 0.6)$. The trajectories of the vortex above an infinite resting lower layer and above a strong slope $s = 0.015$ are very close for $R = 30$ km and $R = 40$ km independently of the initial lower-layer streamfunction or slope orientation. They exhibit slight differences when $R = 80$ km (the final westward displacement are 235, 220, and 180 km for the reduced-gravity model, the finite depth/strong

north–south slope with $\pi_2 = 0$ and $\psi_2 = 0$, respectively), but remain quite close in comparison with the flat bottom case.

[Notice that, in [Fig. 7](#), the total trajectory for the flat-bottom experiment did not fit in the plot and that the final vortex position was $(x, y) = (-380, -430)$ km.] This result is somewhat surprising as for such radii, δ_{TRW} and δ_{NL} are not small and the topographic Rossby waves have a rather strong signature in the upper layer. We thus expected a non-negligible influence on the development of the beta gyre and a subsequent effect on the vortex propagation. That the topographic Rossby waves have no effect on the vortex displacement may be associated with their rather rapid propagation. Indeed, the beta gyre development timescale is τ_1 , which is much bigger than τ_2 , the timescale associated with the topographic Rossby waves. Thus, even though these latter have a strong instantaneous signal, their effect, when averaged over τ_1 , can be quite small.

[Figure 8](#) represents the upper-layer potential vorticity anomaly π_1 evolution at time $t = 0, 50, 100,$ and 150 days for the reduced gravity case and $R = 30$ km. Notice the development of Rossby waves and the general westward displacement. [Figure 9](#) compares the upper-layer potential vorticity anomaly after 150 days for a vortex with a radius $R = 30$ km in the reduced-gravity model ([Fig. 9a](#)), the finite depth/strong north–south slope, $(s_x, s_y) = (0, 0.015)$, and either $\psi_2 = 0$ ([Fig. 9b](#)) or $\pi_2 = 0$ ([Fig. 9c](#)), and finally the finite depth/strong east–west slope, $(s_x, s_y) = (0.015, 0)$, with $\psi_2 = 0$ ([Fig. 9d](#)). Each model yields rather close evolutions, whatever the initial lower-layer velocity field or slope orientation.

[Figure 10](#) is the same as [Fig. 9](#) except that the vortex radius is now $R = 80$ km and [Fig. 10e](#) represents the evolution above a flat bottom. Some discrepancies between the different models become clearer in the Rossby wave field and vortex structure but the vortex remains stable above an infinite lower layer or steep topography. This is not the case above a flat bottom where the vortex exhibits an unstable behavior and has a much larger propagation speed (see [Fig. 10e](#)).

b. Unstable regime

When δ_{NL} is increased beyond 1, the vortex above a strong slope is apparently unstable and dispersed by topographic Rossby waves.

[Figure 11](#) illustrates the $\delta_{\text{NL}} \geq 1$ case. It represents π_1 after 300 days for an initial radius $R = 120$ km [$(\delta_{\text{disp}}, \delta_{\text{TRW}}, \delta_{\text{NL}}) \approx (1.2, 0.7, 1.2)$], in the reduced-gravity case ([Fig. 11a](#)) or the finite depth with a strong north–south ([Fig. 11b](#)) or east–west ([Fig. 11c](#)) slope and $\psi_2 = 0$ initially. The vortex remains stable above an infinite lower layer, but in the presence of a strong bottom slope it is unable to maintain its coherence in this case. This is quite clear with a north–south slope ([Fig. 11b](#)) where the vortex does not seem to move and is dispersed by topographic Rossby waves. The east–west slope case is closer to the reduced-gravity case, but some strong differences can be seen in the streamfunction field, which exhibits strong meanders and small-scale structures due to several instability period and subsequent scattering. As in this regime topographic Rossby waves have a strong signature in the upper layer ($\delta_{\text{TRW}} = 0.7$), it is not surprising to see differences between two different slope orientations.

We have tested for the evolution of this vortex above a strong east–west or north–south slope and without planetary beta effect and found that it was unstable. As a compensated vortex above a slope is a steady state on the f plane, one can investigate the linear stability properties of the vortex and look for stable or unstable eigenmodes. But, to our knowledge, there does not exist any theory for the stability of an isolated compensated vortex over a slope in an unbounded domain, and previous studies have, as is the case in this one, relied on scaling analysis. For instance, [La Casce \(1998\)](#) based his analysis on the dispersion coefficient δ_{disp} . He found that when $\delta_{\text{disp}} \leq 0.5$ or so, a compensated surface vortex is stabilized to weak perturbations above a strong bottom slope.

6. Discussion

In this paper, we have studied the evolution of a quasigeostrophic, surface-intensified vortex and sought under which circumstances a reduced-gravity model is valid when we take into account a strong bottom slope. We found that the reduced-gravity model can be adequate for oceanic situations when the vortex evolves above a steep enough bottom topography and provided δ_{NL} and $\delta_{\text{TRW}} < 0.3$ (which corresponds to vortex radii smaller than 50 km for a maximum vorticity $\Omega_1 = 0.3f$ and for the stratification used in this paper). This result is independent of the slope orientation. When the vortex radius is increased, some differences appear as the topographic Rossby wave signature becomes strong in the surface layer, but both configurations apparently yield similar vortex trajectories and stability property up to $\delta_{\text{NL}} \approx 1$ ($R \approx$

100 km). This could be due to the rapid propagation of topographic waves in comparison with the beta-gyre development timescale, the former having a negligible mean influence on the latter. When $\delta_{NL} > 1$, the vortex becomes unstable, loses its coherence and is dispersed by topographic Rossby waves. We believe that these conclusions are not sensitive to the vortex initial shape (a Gaussian decay in this paper) as long as the vortex is isolated (fast decay away from the core: see [Morel and McWilliams 1997](#)) and the definitions of the vortex radius and strength consistent with our definitions (radius at which the velocity is maximum and vorticity maximum respectively). For instance, one should keep in mind that the previous results on the sensitivity of the vortex behavior to its radius were obtained for a constant maximum vorticity Ω_1 . These are the main results of this paper.

When the reduced-gravity regime is valid, we have seen that, after a while, some differences can appear when we compare the evolution of a surface-intensified vortex in a reduced gravity and in a finite depth but steep topography configuration. These differences are due to an energy loss of the vortex in the finite depth model as, in this case, the vortex displacement generates a motion in the lower layer. In the long term, this can lead to substantial differences between the vortex structures in both models. To avoid these discrepancies, the reduced-gravity model should be periodically reinitialized with the upper-layer streamfunction of the finite depth/steep topography experiment, with a period much shorter than the rate of decay. We have been unable to calculate this rate in the general case, but an estimate can be obtained under some assumptions (see appendix B). [Equation \(B4\)](#) and the numerical experiment presented here show that the decay is slow enough to be negligible if we consider the vortex evolution for 100–150 days.

As far as application to oceanic situations is concerned, the weakest point of this study relies on the use of a QG model together with coherent strong vortices and steep bottom topography. Indeed, for the quasigeostrophic model to be valid, the Rossby number must be small and the layer depth must not change too much over the horizontal scale R , which yields, for the depth variation associated with the bottom topography and with our notation, $Ro = U/fR \ll 1$ and $H_2/sR \ll 1$ (see [Cushman-Roisin 1994](#), chapter 6: 77–95, chapter 15: 204–224). The Rossby number in our experiments is $Ro \approx \Omega_1/2f = 0.15$, which is reasonable. But the second criterion yields, for $H_2 = 3500$ m and $s = 0.015$, $R \ll 240$ km. This criterion is roughly satisfied when $R < 50$ km, and we thus believe our results on the similarity between steep topography and the reduced-gravity model are also valid in a two-layer shallow-water model. It is, however, not satisfied in the experiments where we have considered $R = 80$ – 120 km. Even though a comparison with a full shallow-water model would be interesting, we do not expect strong qualitative differences between both models as far as topographic Rossby wave signature in the upper layer or vortex stability are concerned.

In addition, the unphysical situations described above (strong layer thickness changes or even bottom topography larger than the fluid depth for large vortex radii) are also associated with the fact that, for the sake of simplicity, we have only considered a constant bottom slope in this paper. We believe that our conclusions could be similar above a randomlike topography with steep seamounts of small scale in comparison with the vortex size and for which the quasigeostrophic assumptions are not violated. In this case the topography should indeed also disperse the motion in the lower layer and act so as to maintain the lower layer motion weak (G. M. Reznik 1995, personal communication).

Many field observations have shown strong interaction of surface intensified vortices, such as Agulhas eddies, Gulf Stream rings or eddies in the Gulf of Mexico, with steep topography (Walvis ridge, continental slopes, or a variable but steep bottom topography). According to our analysis, these vortices should rapidly evolve into a compensated state where there is no motion in the lower layer and, if their radius is small enough, evolve as in a reduced-gravity model. If their size is large, they should undergo a stalling period in comparison with the flat-bottom case, and for very large radii ($R > 100$ km) they should become unstable and be dispersed by topographic Rossby waves. [Kamenkovich et al. \(1996\)](#) studied the effect of a steep ridge (Walvis ridge) on the behavior of large-scale vortices (Agulhas eddies). They found that the deep motion undergoes dispersion, the vortex thus becoming compensated, and that the eddy trajectory was deflected westward. [Byrne et al. \(1995\)](#) analyzed Geosat data and found that Agulhas eddies usually slow down when they cross the Walvis Ridge. Both Kamenkovich et al. and Byrne et al. results can be explained with our results and correspond to the expected behavior for a vortex with an intermediate radius ($0.3 \leq \delta_{NL} \leq 1$), $R \approx 60$ to 100 km, for the stratification and bottom slope used in [section 5](#) and a maximum vorticity $\Omega_1 \approx 0.3f$.

Let us also mention that this study could have some implications as far as large-scale general circulation modeling is concerned. Indeed, in coarse resolution models, the bottom topography is smoothed. We have shown that steep topography is similar to a scale selective dissipation mechanism and this could be added in general circulation models to take into account small scale “roughness” of the bottom topography. However, we have only considered vortices and a two-layer quasigeostrophic model in this paper. A lot of work would be necessary to assess the vertical extent of this effect, its influence on more general currents, or the way it could be parameterized.

Finally, despite that we have only considered a two-layer model, these conclusions can also apply to intermediate mesoscale vortices in a three-layer model, provided the Froude numbers $F_f R^2$ are calculated taking into account the

stratification at the vortex level. This was indeed confirmed both by three-layer numerical studies and experiments in rotating tanks on intermediate depth vortices (see [Morel 1995](#)).

Acknowledgments

We wish to particularly thank Joseph La Casce and Xavier Carton for their help during this study. Their advice and comments greatly improved this manuscript. Part of this study was made when Yves Morel was a Ph.D. student at IMG (Institut de Mécanique de Grenoble). He would like to thank Christian Le Provost and Sophie Valcke for the many fruitful conversations during this period, and Gabriel Chabert d’Hières and René Carcel for participating in intriguing experiments using a rotating tank that served to identify the issues addressed here. This research was supported by the French Navy Hydrographic and Oceanographic Service (SHOM).

REFERENCES

- Abramowitz, M., and I. Stegun, 1972: *Handbook of Mathematical Functions*. Dover, 1046 pp..
- Byrne, D., A. Gordon, and W. Haxby, 1995: Agulhas eddies: A synoptic view using Geosat ERM data. *J. Phys. Oceanogr.*, **25**, 902–917.. [Find this article online](#)
- Chassignet, E., and B. Cushman-Roisin, 1991: On the influence of a lower layer on the propagation of nonlinear oceanic eddies. *J. Phys. Oceanogr.*, **21**, 939–957.. [Find this article online](#)
- Cushman-Roisin, B., 1994: *Introduction to Geophysical Fluid Dynamics*. Prentice-Hall, 320 pp..
- Flierl, G., 1977: The application of linear quasi-geostrophic dynamics to Gulf Stream rings. *J. Phys. Oceanogr.*, **7**, 365–379.. [Find this article online](#)
- , 1984: Rossby wave radiation from a strongly nonlinear warm eddy. *J. Phys. Oceanogr.*, **14**, 47–58.. [Find this article online](#)
- , 1988: On the instability of geostrophic vortices. *J. Fluid Mech.*, **97**, 349–388..
- Kamenkovich, V., Y. Leonov, D. Byrne, A. Gordon, and D. Nechaev, 1996: On the influence of bottom topography on the Agulhas eddy. *J. Phys. Oceanogr.*, **26**, 892–912.. [Find this article online](#)
- Killworth, P., 1983: On the motion of isolated lenses on a beta-plane. *J. Phys. Oceanogr.*, **13**, 368–376.. [Find this article online](#)
- La Casce, J., 1998: A geostrophic vortex over a slope. *J. Phys. Oceanogr.*, **28**, 2362–2381.. [Find this article online](#)
- McWilliams, J., and G. Flierl, 1979: On the evolution of isolated lenses on a beta-plane. *J. Phys. Oceanogr.*, **9**, 1155–1182.. [Find this article online](#)
- Morel, Y., 1995: Etude des déplacements et de la dynamique des tourbillons géophysiques. Application aux Meddies. Thèse de doctorat de l’Université Joseph Fourier, 155 pp. [Available from Université Joseph Fourier, BP53X, 38041 Grenoble Cedex, France.].
- , and J. McWilliams, 1997: Evolution of isolated interior vortices in the ocean. *J. Phys. Oceanogr.*, **27**, 727–748.. [Find this article online](#)
- Mory, M., 1985: Integral constraints on bottom and surface isolated eddies. *J. Phys. Oceanogr.*, **15**, 1433–1438.. [Find this article online](#)
- , M. Stern, and R. Griffiths, 1987: Coherent baroclinic eddies on a sloping bottom. *J. Fluid Mech.*, **183**, 45–62..
- Nof, D., 1981: On the beta induced movement of isolated baroclinic eddies. *J. Phys. Oceanogr.*, **11**, 1662–1672.. [Find this article online](#)
- Orszag, 1971: Numerical simulation of incompressible flows within simple boundaries. I. Galerkin (spectral) representations. *Stud. Appl. Math.*, 293–328..
- Pedlosky, J., 1987: *Geophysical Fluid Dynamics*. Springer-Verlag, 710 pp..
- Reznik, G. M., and W. K. Dewar, 1994: An analytical theory of distributed axisymmetric barotropic vortices on the β -plane. *J. Fluid Mech.*, **269**, 301–321..
- Sutyrin, G. G., and G. Flierl, 1994: Intense vortex motion on the beta-plane: Development of the beta gyres. *J. Atmos. Sci.*, **51**, 773–790.. [Find this article online](#)

—, and Y. Morel, 1997: Intense vortex motion in a stratified fluid on the beta-plane: An analytical theory and its validation. *J. Fluid Mech.*, **336**, 203–220..

Swaters, G., and G. Flierl, 1991: Dynamics of ventilated coherent cold eddies on a sloping bottom. *J. Fluid Mech.*, **223**, 565–587..

Thierry, V., 1996: Etude de l'interaction tourbillon-topographie en milieu stratifié. Rapport de stage de D. E. A. de l'Université de Bretagne Occidentale, 31 pp. [Available from EPSHOM-CMO, BP 426, 29275, Brest, Cedex, France.].

Verron, J., and S. Valcke, 1994: Scale dependent merging of baroclinic vortices. *J. Fluid Mech.*, **264**, 81–106..

APPENDIX A

7. Lower Layer Motion

Under the assumption that dispersion dominates the lower-layer dynamics, all nonlinear terms can be neglected in [Eq. \(4b\)](#), which becomes

$$\partial_t(\zeta_2 - F_2 \psi_2) + \beta_{2,y} \partial_x \psi_2 - \beta_{2,x} \partial_y \psi_2 = -F_2 \partial_t \psi_1. \quad (\text{A1})$$

Let us then solve [\(A1\)](#) and calculate ψ_2 as a function of ψ_1 . To do so, we consider a spatial Fourier transform of [\(A1\)](#):

$$\partial_t \psi_2 + \left(\frac{i\beta_{2,x}l}{K^2 + F_2} - \frac{i\beta_{2,y}k}{K^2 + F_2} \right) \psi_2 = \frac{F_2 \partial_t \psi_1}{K^2 + F_2}, \quad (\text{A2})$$

where (k, l) are the east–west and north–south wavenumbers, $K^2 = k^2 + l^2$, and

$$\hat{G} = \iint e^{-i(kx+ly)} G(x, y, t) dx dy$$

$$G = \frac{1}{4\pi^2} \iint e^{i(kx+ly)} \hat{G}(k, l, t) dk dl,$$

where \hat{G} is the Fourier transform of G .

[Equation \(A2\)](#) is readily solved and the solution is

$$\psi_2 = \exp\left(it \frac{\beta_{2,y}k - \beta_{2,x}l}{K^2 + F_2}\right)$$

$$\times \int_0^t \frac{F_2 \partial_{t'} \psi_1}{K^2 + F_2} \exp\left(it' \frac{\beta_{2,y}k - \beta_{2,x}l}{K^2 + F_2}\right) dt'. \quad (\text{A3})$$

Let us now assume that over a reasonable time period the upper-layer vortex is steadily propagating westward for the sake of simplicity:

$$\hat{\psi}_1 = \hat{\psi}_1^o(k, l) e^{-ikCt},$$

where $\hat{\psi}_1^o$ is the Fourier transform of ψ_1 at $t = 0$ and C is the propagation speed of the structure. In this case we find

$$\times \left[\exp(-ikCt) - \exp\left(it \frac{\beta_{2,y}k - \beta_{2,x}l}{K^2 + F_2}\right) \right]. \quad (\text{A4})$$

This equation shows that there are two timescales involved in the evolution of ψ_2 , a slow one associated with the forcing by the upper-layer vortex displacement and subsequent stretching and a rapid one associated with the bottom topography. Both parts have the same order of magnitude, which will be evaluated by calculating ψ_2 at the center of the upper-layer vortex where the stretching is maximum, ($x = Ct, y = 0$) and considering the main axisymmetric part of ψ_1^o only. Using the inverse Fourier transform, we get

$$\psi_2^o = \frac{1}{4\pi^2} \iint F_2 C k \psi_1^o \frac{1 - \exp\left[it \left(kC + \frac{\beta_{2,y}k - \beta_{2,x}l}{K^2 + F_2}\right)\right]}{kC(K^2 + F_2) + \beta_{2,y}k - \beta_{2,x}l} dk dl.$$

This integral can be calculated using polar coordinates $k = K \cos\theta$, $l = K \sin\theta$ and defining α so that

$$\cos\alpha = \frac{C(K^2 + F_2) + \beta_{2,y}}{\{\beta_{2,x}^2 + [\beta_{2,y} + C(F_2 + K^2)]^2\}^{1/2}}$$

$$\sin\alpha = \frac{\beta_{2,x}}{\{\beta_{2,x}^2 + [\beta_{2,y} + C(F_2 + K^2)]^2\}^{1/2}}.$$

Using the integral definition of the Bessel function $J_0(z) = (2\pi)^{-1} \int_0^{2\pi} e^{z\cos\theta} d\theta$ (see [Abramowitz and Stegun 1972](#)), we get

$$\psi_2^o = \frac{1}{2\pi} \int_0^\infty F_2 C \frac{K \psi_1^o}{\{\beta_{2,x}^2 + [\beta_{2,y} + C(F_2 + K^2)]^2\}^{1/2}} \cos\alpha F(K, t) dK,$$

where

$$F(K, t) = 1 - J_0\left(\frac{\{\beta_{2,x}^2 + [(K^2 + F_2)C + \beta_{2,y}]^2\}^{1/2}}{K^2 + F_2} t\right).$$

As $\psi_1^o = (2\pi)^{-1} \int_0^\infty \hat{\psi}_1^o K dK$, $J_0(z) \rightarrow 0$ at infinity, $C \approx R/\tau_1 = \beta_1 R^2/(2 + F_1 R^2)$ and, for a strong bottom slope, $\beta_2 \gg C(K^2 + F_2)$ this equation can be used to give an estimated upper bound on ψ_2^o :

$$\psi_2^o = \frac{\beta_1}{\beta_2} \frac{F_2 R^2}{2 + F_1 R^2} \psi_1^o. \quad (\text{A5})$$

APPENDIX B

8. Vortex Decay

If the lower layer is at rest, the energy of the structure is

$$E_{\text{redg}} = \iint_{R^2} \|\nabla\psi_1\|^2 + F_1\|\psi_1\|^2 dx dy. \quad (\text{B1})$$

This quantity is conserved if the lower layer is infinitely deep, but when the lower-layer depth is finite and on the β plane, E_{redg} is not conserved as the upper vortex displacement generates topographic Rossby waves and the lower layer can no longer be considered at rest. We can calculate the evolution equation for E_{redg} in the finite lower-layer depth case by multiplying Eq. (4a) by ψ_1 and integrating through the whole horizontal domain. This yields (with the assumption that ψ_1 and ψ_2 rapidly tend to zero at infinity)

$$\partial_t E_{\text{redg}} = \iint_{R^2} F_1 \psi_1 \partial_t \psi_2 dx dy. \quad (\text{B2})$$

To estimate the decay timescale associated with the generation of Rossby waves and motion in the lower layer, we must derive an order of magnitude for the right-hand term of (B2) and evaluate $D = \iint_{R^2} F_1 \psi_1 \partial_t \psi_2 dx dy$. This involves both the slow and rapid parts of ψ_2 and their correlation with ψ_1 . If we assume that the correlation is maximum for the rapid part of ψ_2 and is concentrated in the vicinity of the vortex core, we get

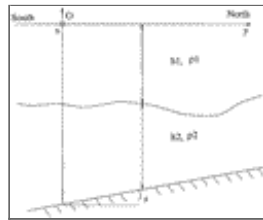
$$\begin{aligned} O(D) &\simeq F_1 O(\psi_1) O(\psi_2) R^2 / \tau_2 \\ &= F_1 \frac{\Omega_1 R^2}{2} \frac{\Omega_2 R^2}{2} R^2 / \tau_2. \end{aligned} \quad (\text{B3})$$

This thus yields a rough estimate for the decay rate T_{decay}

$$\begin{aligned} T_{\text{decay}} &\simeq \frac{E_{\text{redg}}}{O(D)} \\ &= \frac{(1 + F_1 R^2)(2 + F_1 R^2)(2 + F_2 R^2)}{F_1 R^2 F_2 R^2} \frac{1}{\beta_1 R}. \end{aligned} \quad (\text{B4})$$

It is worth noticing that, as we have assumed that the upper-vortex behavior was not influenced by the lower layer, the rate of decay does not depend on the bottom slope. Indeed, if the lower-layer dispersion is rapid enough, the factor limiting the decay is the rate at which the upper vortex transfers energy to the lower layer via stretching, which only depends on the upper vortex displacement speed, interface deviations, and stratification.

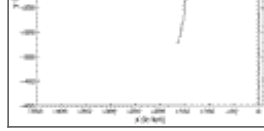
Figures



[Click on thumbnail for full-sized image.](#)

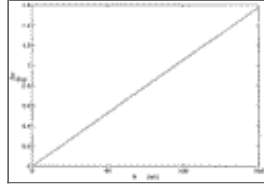
Fig. 1. Model description.





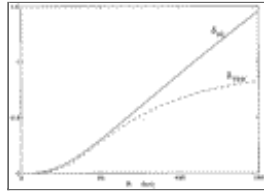
Click on thumbnail for full-sized image.

Fig. 2. Vortex trajectories for $H_1 = H_2 = 1500$ m, $g' = 0.01$, $R = 40$ km, $\Omega_1 = 0.3f$ and $s = 0$ (dotted), $(s_x, s_y) = (0, 0.01)$ (dashed), $(s_x, s_y) = (0.01, 0)$ (where circles indicate the vortex position every 10 days) and in the reduced gravity case (plain). Each curve represent vortex trajectories for 150 days. Notice the similarity between the strong slope and the reduced gravity cases.



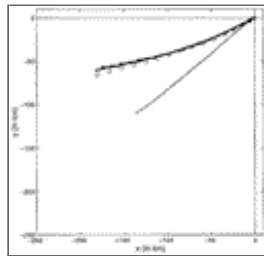
Click on thumbnail for full-sized image.

Fig. 3. Lower-layer dispersion coefficient, $\delta_{\text{disp}} = F_2 \Omega_1 H_2 R / fs$, as a function of the vortex radius R for $H_1 = 500$ m, $H_2 = 3500$ m, $g' = 0.01$, $\Omega_1 = 0.3f$, and $s = 0.015$. Dispersion occurs up to $\delta_{\text{disp}} \approx 1$ or so.



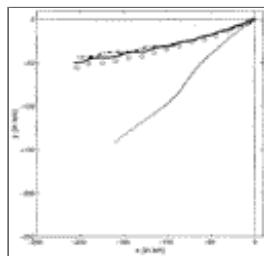
Click on thumbnail for full-sized image.

Fig. 4. Plot of δ_{TRW} (dashed) and δ_{NL} (plain) as a function of the vortex radius R for the same background stratification and vortex strength as in Fig. 3. These parameters measure the influence of the lower layer on the evolution of the upper vortex.



Click on thumbnail for full-sized image.

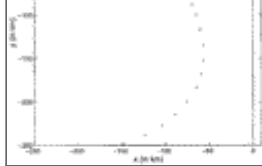
Fig. 5. Vortex center (upper layer streamfunction maximum) trajectories in a reduced gravity model (plain line), a finite depth without topography (dotted), a finite depth with a strong topography, and $(s_x, s_y) = (0, 0.015)$, $\pi_2 = 0$ initially (dash-dotted) $(s_x, s_y) = (0, 0.015)$, $\Psi_2 = 0$ initially (dashed) or $(s_x, s_y) = (0.015, 0)$, $\Psi_2 = 0$ initially (circles every 10 days). $H_1 = 500$ m, $H_2 = 3500$ m, $g' = 0.01$, $\Omega_1 = 0.3f$ and the vortex radius is $R = 30$ km. Each curve represent vortex trajectories for 150 days.



Click on thumbnail for full-sized image.

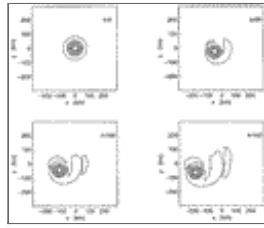
Fig. 6. Same as Fig. 5 except for $R = 40$ km.





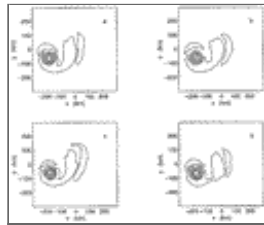
[Click on thumbnail for full-sized image.](#)

Fig. 7. Same as [Fig. 5](#) except for $R = 80$ km.



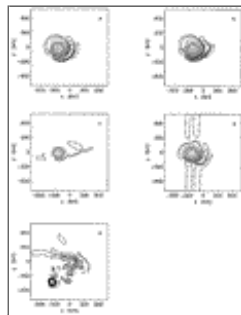
[Click on thumbnail for full-sized image.](#)

Fig. 8. Upper-layer potential vorticity anomaly field ψ_1 at time $t = 0, 50, 100,$ and 150 days in the reduced gravity model for $H_1 = 500$ m, $H_2 = \infty$, $g' = 0.01$, $\Omega_1 = 0.3f$, and the vortex radius is $R = 30$ km.



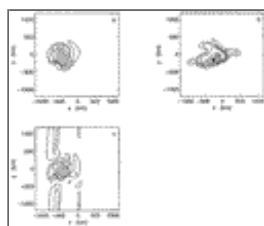
[Click on thumbnail for full-sized image.](#)

Fig. 9. Upper-layer potential vorticity anomaly at $t = 150$ days for a vortex of radius $R = 30$ km and for $H_1 = 500$ m, $H_2 = 3500$ m, $g' = 0.01$, and $\Omega_1 = 0.3f$. Results shown are from the reduced-gravity model (a), finite depth/strong north–south (b) or east–west (d) slope ($s = 0.015$) with $\psi_2 = 0$ initially and finite depth/strong north–south slope with $\pi_2 = 0$ initially (c). The same contour values are used in each plot.



[Click on thumbnail for full-sized image.](#)

Fig. 10. Same as [Fig. 9](#) except that $R = 80$ km and (e) is the upper-layer streamfunction for an evolution above a flat bottom and with $\psi_2 = 0$ initially.



[Click on thumbnail for full-sized image.](#)

Fig. 11. Upper-layer potential vorticity anomaly at $t = 300$ days for a vortex of radius $R = 120$ km and for $H_1 = 500$ m, $H_2 = 3500$ m, $g' = 0.01$, and $\Omega_1 = 0.3f$. Results shown are from the reduced-gravity model (a) and finite depth/strong north–south, (b) or

east–west (c) slope model with $\Psi_2 = 0$ initially.

¹ Here, barotropic means that the vortex structure is independent of depth.

Corresponding author address: Dr. Yves Morel, EPSHOM-CMO, B.P. 426, 29275 Brest, Cedex, France.

E-mail: morel@shom.fr

top ▲



© 2008 American Meteorological Society [Privacy Policy and Disclaimer](#)
Headquarters: 45 Beacon Street Boston, MA 02108-3693
DC Office: 1120 G Street, NW, Suite 800 Washington DC, 20005-3826
amsinfo@ametsoc.org Phone: 617-227-2425 Fax: 617-742-8718
[Allen Press, Inc.](#) assists in the online publication of *AMS* journals.